



NASF SURFACE TECHNOLOGY WHITE PAPERS

88 (9), 10-14 (June 2024)

9th Quarterly Report
January-March 2024
AESF Research Project #R-123

Electrochemical Manufacturing for Energy Applications

by
*Majid Minary Jolandan**
Department of Mechanical Engineering
The University of Texas at Dallas
Richardson, Texas, USA

Editor's Note: *The NASF-AESF Foundation Research Board selected a project on electrodeposition toward developing low-cost and scalable manufacturing processes for hydrogen fuel cells and electrolysis cells for clean transportation and distributed power applications. This report covers the ninth quarter of work, from January through March 2024.*

1. Introduction

Hydrogen has been identified by the US government as a key energy option to enable full decarbonization of the energy system.¹ The US government has recently initiated a significant investment in the Hydrogen Economy, which is detailed in the recent "Road Map to a US Hydrogen Economy: reducing emissions and driving growth across the nation" report. In June 2023, the first ever "US National Clean Hydrogen Strategy and Roadmap" was published.² On Nov. 15, 2021, President Biden signed the Bipartisan Infrastructure Law (BIL). The BIL authorizes appropriations of \$9.5B for clean hydrogen programs for the five-year period 2022-2026, including \$1B for the Clean Hydrogen Electrolysis Program. In alignment with the BIL and the mission of Hydrogen Energy "Earthshot" to reach the goal of \$1 per 1 kg in 1 decade ("1 1 1"), the US is projected to invest in priority areas that will advance domestic manufacturing and recycling of clean hydrogen technologies.

Solid oxide electrolyzer cells (SOECs) are energy storage units that produce storable hydrogen from electricity (more recently increasingly from renewable sources) and water (electrolysis of water).³ The majority (~95%) of the world's hydrogen is produced by the steam methane reforming (SMR) process that releases the greenhouse gas carbon dioxide.⁴ Electrolytic hydrogen (with no pollution) is more expensive compared to hydrogen produced using the SMR process. Investments in manufacturing and process development and increasing production scale and industrialization will reduce the cost of electrolytic hydrogen. Based on the recent DOE report, with the projected growth of the hydrogen market, the US electrolyzer capacity will have to increase by 20% compound annual growth from 2021 to 2050, with an annual manufacturing requirement of over 100 GW/yr. Given the complex structure and stringent physical and functional requirements of SOECs, additive manufacturing (AM) has been proposed as one potential technological path to enable low-cost production of durable devices to achieve economies of scale, in conjunction with the ongoing effort on traditional manufacturing fronts.⁵ Recently (2022), the PI published an article on challenges and opportunities in AM of SOCs,⁵ in which a comprehensive review of the state-of-the-art in this field is presented.

In this work, we aim to contribute to such effect of national interest to enable the hydrogen economy through development of manufacturing processes for production of low cost, durable and high efficiency solid oxide fuel cells (SOFCs) and SOECs.

* Corresponding author:

Dr. Majid Minary Jolandan
Department of Mechanical Engineering
The University of Texas at Dallas
800 West Campbell Road
Richardson, TX 75080-3021
Office: ECSW 4.355H
Phone: (972) 883-4661
Email: majid.minary@utdallas.edu

NASF SURFACE TECHNOLOGY WHITE PAPERS 88 (9), 10-14 (June 2024)

2. Summary of Accomplishments (January-March 2024 Quarter)

In this period, we followed our work on 3D printing anode support for solid oxide fuel cells, SOFC (or cathode for solid oxide electrolyzers, SOEC). We focused on the mechanical properties of 3D printed yttria-stabilized zirconia (YSZ) using a four-point bending test. We then conducted a statistical analysis to characterize the flexural strength of porous 3D printed YSZ.

3. Activity

While porosity is essential for facilitating gas transport within the electrodes, it can also substantially impact the mechanical properties of ceramics.¹ This is particularly important as the electrodes often serve as the support structure, needing to endure various internal and external mechanical loads. To address the concerns of both optimal porosity and mechanical properties of the anode structure (in anode-supported SOFCs), a sintering temperature of 1150°C with a porosity of ~33% (RD ~67%) was chosen for further investigation (Figure 1).

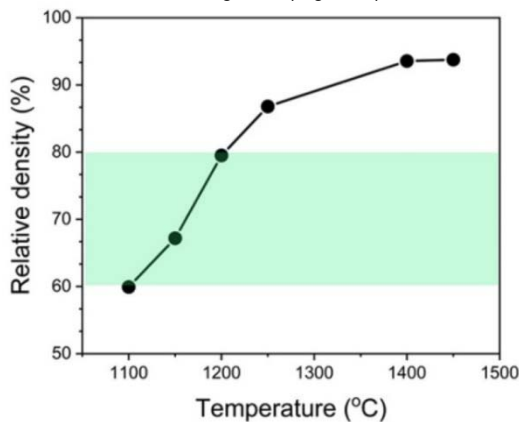


Figure 1 - Relative density (RD) of 3D printed porous YSZ at different sintering temperatures.

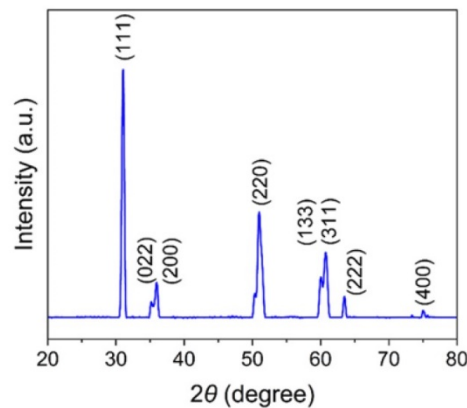


Figure 2 - XRD pattern of porous 3D printed 3YSZ sintered at 1150°C.

X-ray diffraction (XRD) analysis was employed to identify the crystalline phases present in the porous 3D printed YSZ sintered at 1150°C (Figure 2). The diffractogram revealed the predominant presence of the tetragonal phase, evidenced by characteristic peaks at 2θ values of $\sim 31^\circ$, $35\text{-}36^\circ$, $50\text{-}51^\circ$, $59\text{-}64^\circ$ and $\sim 75^\circ$. Notably, no cubic phase was detected, consistent with the tetragonal phase reported for dense YSZ in similar studies.²⁻⁵

To investigate the mechanical properties of the porous 3D printed YSZ component, flexural tests at room temperature were performed (Figure 3), using a four-point bending test. The porous beams displayed a range of flexural strength between ~ 31 and ~ 40 MPa, with an average flexural strength of 35.6 ± 2.7 MPa.

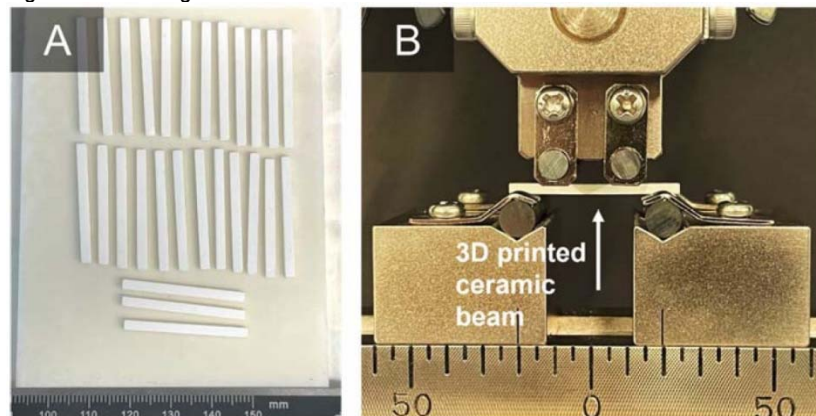


Figure 3 - (A) 3D printed 3YSZ beam sintered at 1150°C, (B) four-point bending test.

NASF SURFACE TECHNOLOGY WHITE PAPERS 88 (9), 10-14 (June 2024)

Cai, *et al.*⁶ studied flexural strength of porous 3YSZ manufactured by freeze-casting at two different sintering temperatures, 1200°C and 1300°C, corresponding 46% and 40% porosity. Their findings revealed that increasing the sintering temperature from 1200°C to 1300°C led to a corresponding increase in flexural strength (from 24 MPa to 50 MPa). Riyad, *et al.*⁷ reported a three-point bending flexural strength of ~18 MPa for 8YSZ, fabricated by freeze-casting with a porosity of ~45%. Hu, *et al.*⁸ obtained a compressive strength ranging from ~3 to ~29 MPa for 8YSZ manufactured by a gel-casting process and various sintering temperatures. It should also be noted that the measured strength may vary, based on the measurement method. For instance, in the three-point bending test, a beam is subjected to both shear and bending loads over its entire length, with the maximum bending moment in the mid-span of the beam. In a four-point bending test however, the span of the beam between the two interior loads is shear-free, and under a constant pure bending moment.⁹

Given the probabilistic nature of ceramic failure, such differences in loading and its interaction with processing flaws may result in different strength values. In the case of brittle ceramics, mechanical strength is influenced by the presence of flaws. However, it is important to note that these flaws may not be consistently distributed throughout the samples, and in some cases, they may be clustered unevenly. This uneven distribution of flaws could potentially trigger crack growth during mechanical testing. Consequently, when reporting mechanical strength data for 3D printed ceramic materials, it is crucial to consider this variability, and report statistical analysis.¹⁰

For ceramic materials, the Weibull analysis is the preferred method, because of the stochastic nature of failure in these materials, produced by process defects and porosity. The probability of failure is mathematically expressed as:

$$P_f = 1 - \exp\left(-\left(\frac{\sigma}{\sigma_0}\right)^m\right),$$

where m is the Weibull modulus, and σ_0 is the characteristic strength.^{7,9} The Weibull modulus is a shape parameter that converts a specimen's likelihood of failure over a range of strength levels. For the analysis, the flexural strength values of the specimens were ranked in ascending order and assigned a corresponding probability of failure using $P_f = (i - 0.5)/N$, where P_f is the rank of the i_{th} specimen and N is the total number of tested specimens. Probabilities of flexural strengths are reported in terms of $\ln\left(\ln\left(\frac{1}{1-P_f}\right)\right)$ and $\ln(\sigma)$. The Weibull modulus, m , was obtained by fitting a straight line as the slope of the Weibull plot of $\ln\left(\ln\left(\frac{1}{1-P_f}\right)\right)$ against $\ln(\sigma)$. A Weibull plot for flexural strength is shown in Figure 4. A modulus of $m = 5.3$ and a characteristic strength of 36.4 MPa was obtained for porous 3D printed YSZ beams.

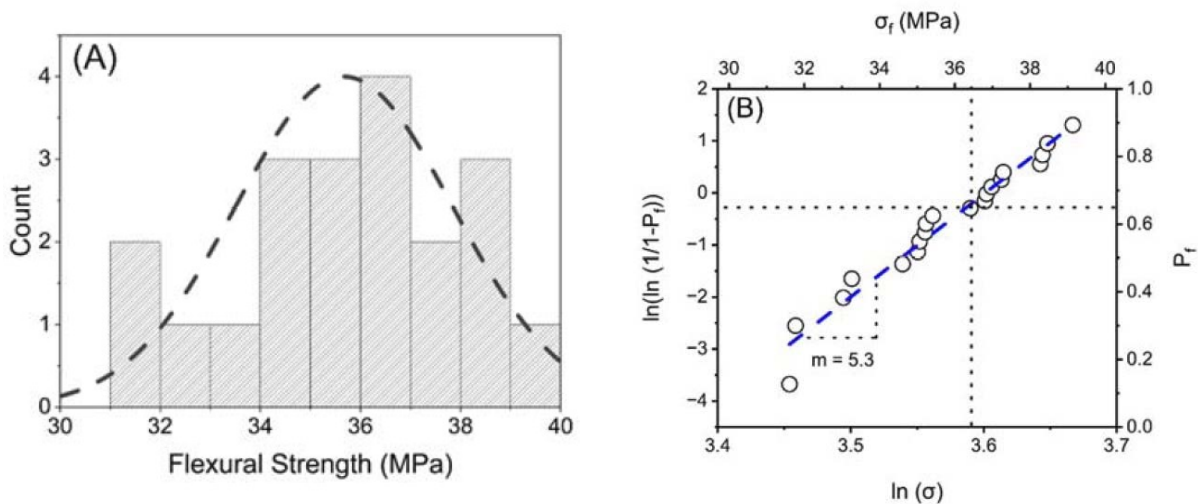


Figure 4 - (A) Distribution of the flexural strength of porous YSZ beams; (B) The Weibull analysis and characteristic strength of porous 3D printed YSZ beams.

NASF SURFACE TECHNOLOGY WHITE PAPERS 88 (9), 10-14 (June 2024)

For engineered ceramics, the Weibull modulus is reported to be in a range of 5 to 10.¹¹ Fan, *et al.*¹² reported that for porous brittle ceramics, the value of the Weibull modulus was in the range of 4 to 11. For 3D printed polymer-derived ceramics, freeze-cast 8YSZ with a porosity of ~45%, and 3D printed alumina, Weibull moduli of 3.7, 5.7 and 3.9, respectively, were recently reported.^{7,9,10} Each printing technology (*e.g.*, stereolithography, freeze-casting and DLP) introduces unique manufacturing flaws and affects the overall material microstructure. Printing parameters such as layer thickness, printing speed and post-processing steps also influence the Weibull modulus.¹³

Our research currently focuses on investigating the thermal shock behavior of 3D printed porous YSZ with the porosity of approximately 33%.

4. References

1. C.L. Cramer, *et al.*, "Additive manufacturing of ceramic materials for energy applications: Road map and opportunities," *J. Eur. Ceram. Soc.*, 42 (7), 3049-3088 (2022); <https://doi.org/10.1016/j.jeurceramsoc.2022.01.058>.
2. R. He, *et al.*, "Fabrication of complex-shaped zirconia ceramic parts via a DLP-stereolithography-based 3D printing method," *Ceram. Int.*, 44 (3), 3412-3416 (2018); <https://doi.org/10.1016/j.ceramint.2017.11.135>.
3. D. Komissarenko, S. Roland, B.S.M. Seeber, T. Graule and G. Blugan, "DLP 3D printing of high strength semi-translucent zirconia ceramics with relatively low-loaded UV-curable formulations," *Ceram. Int.*, 49 (12), 21008-21016 (2023); <https://doi.org/10.1016/j.ceramint.2023.03.236>.
4. S.H. Ji, D.S. Kim, M.S. Park and J.S. Yun, "Sintering process optimization for 3YSZ ceramic 3D-printed objects manufactured by stereolithography," *Nanomaterials*, 11 (1), 192 (2021); <https://doi.org/10.3390/nano11010192>.
5. K.-J. Jang, J.-H. Kang, J. G. Fisher and S.-W. Park, "Effect of the volume fraction of zirconia suspensions on the microstructure and physical properties of products produced by additive manufacturing," *Dent. Mater.*, 35 (5), e97–e106 (2019); <https://doi.org/10.1016/j.dental.2019.02.001>.
6. H. Cai, *et al.*, "Flexural strength and elastic modulus of gradient structured YSZ membranes with multi-scale pores," *Ceram. Int.*, 48 (19), Part A, 27931–27941 (2022); <https://doi.org/10.1016/j.ceramint.2022.06.097>.
7. M.F. Riyad, M. Mahmoudi and M. Minary-Jolandan, "Manufacturing and Thermal Shock Characterization of Porous Ytria Stabilized Zirconia for Hydrogen Energy Systems," *Ceramics*, 5 (3), 472–483 (2022); <https://doi.org/10.3390/ceramics5030036>.
8. L. Hu, C.-A. Wang, and Y. Huang, "Porous yttria-stabilized zirconia ceramics with ultra-low thermal conductivity," *J. Mater. Sci.*, 45 (12), 3242–3246 (2010); <https://doi.org/10.1007/s10853-010-4331-9>.
9. A. Myles, A. Griffith, M.F. Riyad, Y. Jiao, M. Mahmoudi and M. Minary-Jolandan, "3D-Printed Ceramics with Aligned Micro-Platelets," *ACS Appl. Eng. Mater.*, 1 (7), 1892–1902 (2023); <https://doi.org/10.1021/acsaenm.3c00223>.
10. M. Mahmoudi, *et al.*, "Three-dimensional printing of ceramics through 'carving' a gel and 'filling in' the precursor polymer," *ACS Appl. Mater. Interfaces*, 12 (28), 31984–31991 (2020); <https://doi.org/10.1021/acsaenm.3c00223>.
11. M.A. Meyers and K.K. Chawla, *Mechanical behavior of materials*, Cambridge University Press, 2008.
12. X. Fan, E.D. Case, F. Ren, Y. Shu and M.J. Baumann, "Part I: Porosity dependence of the Weibull modulus for hydroxyapatite and other brittle materials," *J. Mech. Behav. Biomed. Mater.*, 8, 21–36 (2012);
13. Ö. Keleş, R.E. García and K.J. Bowman, "Stochastic failure of isotropic, brittle materials with uniform porosity," *Acta Mater.*, 61 (8), 2853–2862 (2013); <https://doi.org/10.1016/j.actamat.2013.01.024>.

5. Past project reports

1. Quarter 1 (January-March 2022): Summary: *NASF Report in Products Finishing, NASF Surface Technology White Papers*, 86 (10), 17 (July 2022); Full paper: <http://short.pfonline.com/NASF22Jul1>.
2. Quarter 2 (April-June 2022): Summary: *NASF Report in Products Finishing, NASF Surface Technology White Papers*, 87 (1), 17 (October 2022); Full paper: <http://short.pfonline.com/NASF22Oct2>.
3. Quarter 3 (July-September 2022) Part I: Summary: *NASF Report in Products Finishing, NASF Surface Technology White Papers*, 87 (3), 17 (December 2022); Full paper: <http://short.pfonline.com/NASF22Dec2>.
4. Quarter 3 (July-September 2022) Part II: Summary: *NASF Report in Products Finishing, NASF Surface Technology White Papers*, 87 (4), 17 (January 2023); Full paper: <http://short.pfonline.com/NASF23Jan1>.

NASF SURFACE TECHNOLOGY WHITE PAPERS 88 (9), 10-14 (June 2024)

5. Quarters 4-5 (October 2022-March 2023) Summary: *NASF Report in Products Finishing, NASF Surface Technology White Papers*, 88 (1), 17 (October 2023); Full paper: <http://short.pfonline.com/NASF23Oct1>.
6. Quarter 6 (April-June 2023) Summary: *NASF Report in Products Finishing, NASF Surface Technology White Papers*, 88 (1), 17 (October 2023); Full paper: <http://short.pfonline.com/NASF23Oct2>.
7. Quarter 7 (July-September 2023) Summary: *NASF Report in Products Finishing, NASF Surface Technology White Papers*, 88 (4), 17 (January 2024); Full paper: <http://short.pfonline.com/NASF24Jan1>.
8. Quarter 8 (October-December 2023) Summary: *NASF Report in Products Finishing, NASF Surface Technology White Papers*, 88 (6), 17 (March 2024); Full paper: <http://short.pfonline.com/NASF24Mar2>.

6. About the Principal Investigator for AESF Research Project #R-123



Majid Minary Jolandan is Associate Professor of Mechanical Engineering at The University of Texas at Dallas, in Richardson, Texas, in the Erik Jonsson School of Engineering. His education includes B.S. Sharif University of Technology, Iran (1999-2003), M.S. University of Virginia (2003-2005), Ph.D. University of Illinois at Urbana-Champaign (2006-2010) as well as Postdoctoral fellow, Northwestern University (2010-2012). From 2012-2021, he held various academic positions at The University of Texas at Dallas (UTD) and joined the Faculty at Arizona State University in August 2021. In September 2022, he returned to UTD as Associate Professor of Mechanical Engineering. His research interests include additive manufacturing, advanced manufacturing and materials processing.

Dr. Minary is an Associate Editor for the *Journal of the American Ceramic Society*, an Editorial Board member of *Ceramics* journal and the current chair of the materials processing technical committee of ASME.

Early in his career, he received the Young Investigator Research Program grant from the Air Force Office of Scientific Research to design high-performance materials inspired by bone that can reinforce itself under high stress. This critical research can be used for aircraft and other defense applications, but also elucidates the understanding of bone diseases like osteoporosis. In 2016, he earned the Junior Faculty Research Award as an Assistant Professor at the University of Texas-Dallas – Erik Jonsson School of Engineering.